Received December 27, 2019, accepted January 9, 2020, date of publication January 17, 2020, date of current version January 28, 2020.

Digital Object Identifier 10.1109/ACCESS.2020.2967397

Wideband Circularly Polarized MIMO Antenna for High Data Wearable Biotelemetric Devices

AMJAD IQBAL[1,2], (Student Member, IEEE), AMOR SMIDA[3,4], (Member, IEEE), ABDULLAH J. ALAZEMI[5], (Member, IEEE), MOHAMED I. WALY[3,6], NAZIH KHADDAJ MALLAT[7], (Senior Member, IEEE), AND SUNGHWAN KIM[8]

[1]Centre For Wireless Technology, Faculty of Engineering, Multimedia University, Cyberjaya 63100, Malaysia
[2]Department of Electrical Engineering, CECOS University of IT and Emerging Sciences, Peshawar 25000, Pakistan
[3]Department of Medical Equipment Technology, College of Applied Medical Sciences, Majmaah University, AlMajmaah 11952, Saudi Arabia
[4]Unit of Research in High Frequency Electronic Circuits and Systems, Faculty of Mathematical, Physical, and Natural Sciences of Tunis, Tunis El Manar University, Tunis 2092, Tunisia
[5]Department of Electrical Engineering, Faculty of Engineering and Petroleum, Kuwait University, Kuwait City 13060, Kuwait
[6]Department of Biomedical Engineering and System (formerly), Higher Institute of Engineering, El Shorouk Academy, Al Shorouk City 11511, Egypt
[7]College of Engineering, Al Ain University (AAU), Al Ain 64141, UAE
[8]School of Electrical Engineering, University of Ulsan, Ulsan 44610, South Korea

Corresponding author: Sunghwan Kim (sungkim@ulsan.ac.kr)

This work was supported in part by the Research Program through the National Research Foundation of Korea under Grant NRF-2019R1A2C1005920, and in part by the Deanship of Scientific Research at Majmaah University under Grant R-1441-59.

ABSTRACT This paper presents a miniaturized circularly polarized multiple-input multiple-output (MIMO) antenna for wearable biotelemetric devices. The proposed MIMO antenna consists of four elements, which are placed orthogonally to the adjacent elements. The proposed antenna has a wideband response [10-dB bandwidth of 2210 MHz (fractional bandwidth (FBW) = 92.08%) in free space and 10-dB bandwidth of 2200 MHz (FBW = 91.66%) when worn on human-body], this frequency range covers the important and unlicensed industrial, scientific and medical (ISM) band (2.40–2.48 GHz). The antenna exhibits a wideband 3-dB circularly polarized bandwidth of 1300 MHz (FBW = 54.16%) and 1040 MHz (FBW = 43.33%) in free space and when worn on the body, respectively. The optimized antenna in free space (on-body) has an envelop correlation coefficient (ECC) less than 0.21 (0.23), a diversity gain (DG) greater than 9.77 dB (9.71 dB), a multiplexing efficiency (ME) greater than −0.85 dB (−0.63 dB), and a channel capacity loss (CCL) less than 0.13 bps/Hz (0.13 bps/Hz). The stable radiation, high gain, high efficiency, and good MIMO properties in free space and on human-body make the proposed antenna a suitable choice for use in high data wearable biotelemetric devices.

INDEX TERMS Circularly polarized antenna, MIMO antenna, wearable antenna, wearable biotelemetric devices, wireless body-area networks (WBAN).

I. INTRODUCTION

The design of on-body wearable antennas attracted the attention of researchers worldwide due to their use in interesting applications such as: monitoring health issues, sports activities, military applications and more [1]–[4]. Such antennas are required to be of a low profile, compact size, perform well on a moving body, and most importantly emit low backward radiation. Moreover, it has been well-established that the tissues of the human body have severe impact on the antenna's performance which makes the design of on-body wearable antennas a challenging task. To improve the antenna's performance under such an impact, the use of special structures in the antenna design such as electromagnetic bandgap structures (EBG) [5] and high impedance structures (HIS) [6] was proposed. However, these structures increase the complexity of the antenna and the number of its layers. Another issue to consider is the data rate as biomedical devices nowadays are required to receive and transmit data at a high rate. For instance, modern image sensors can transfer high quality images at a rate of 78 Mbps [7]. In that regard, the selection of the operating band becomes critical, and the ISM band (2.4 GHz) presents a suitable choice for high data rate devices [8]. To reach such high

The associate editor coordinating the review of this manuscript and approving it for publication was Lu Guo.

data rates, many MIMO antennas have recently been proposed for Wireless Body Area Networks (WBAN) [9]–[11]. To achieve compactness, the antennas are densely packed in MIMO systems. The nearby placed MIMO elements induce an effect on each other (mutual coupling [MC]) which is undesirable and therefore impairs the system's performance. The MC can be reduced by either placing the elements far away from each other or by introducing a decoupling structure to the existing system [12]. However, these techniques either enlarge the system size or increase its complexity which is undesirable in a compact system. Another convenient way to keep the elements isolated from each other is to arrange them optimally. The orthogonally arranged MIMO antennas have an almost non-existent MC between them and there is no need to add additional decoupling structures [13]. The MIMO antennas reported for WBANs are mostly linearly polarized and are easily affected by polarization mismatches especially when the wearer changes his/her position.

Circularly polarized (CP) antennas are known to be less impacted by polarization mismatches besides their ability to reduce multi-path distortions. Due to these capabilities, a wideband CP filtering antennas have been developed for biomedical wearable devices in [14]- [15]. In [16], a flexible CP antenna is reported using polydimethylsiloxane (PDMS) and silver nanowires (AgNWs). However, these CP antennas cannot provide high data rates due to their single-input single-output (SISO) topology. Therefore, it is desirable to develop CP MIMO antennas for WBANs to combat polarization mismatches while providing high data rates. Despite their obvious importance, only a few works tackled the design of such antennas [17]–[19]. The designs reported in [17]–[19] demonstrated less performance deterioration due to polarization mismatches compared to their linearly polarized counterparts, however, they all suffered from narrow 3-dB axial ratio bandwidth.

In this paper, we propose a CP MIMO antenna with a wider operational bandwidth and better circular polarization bandwidth for wearable biotelemetric devices. The key advantages of the proposed work are summarized as follows:

- To the best of the authors' knowledge, the presented work performs better than any comparable work in the literature in terms of the 3-dB axial ratio bandwidth. Also, a wide 3-dB axial ratio bandwidth is demonstrated in on-body worn scenario which confirms the suitability of the designed antenna for use in wearable biotelemetric devices and proves its ability to alleviate the severity of the associated polarization mismatch issues. Moreover, the antenna supports high data rates and can resist multi-path fading because of the MIMO architecture.

II. DESIGN METHODOLOGY

The schematic of the proposed wideband four element circularly polarized MIMO antenna is shown in Fig. 1a.

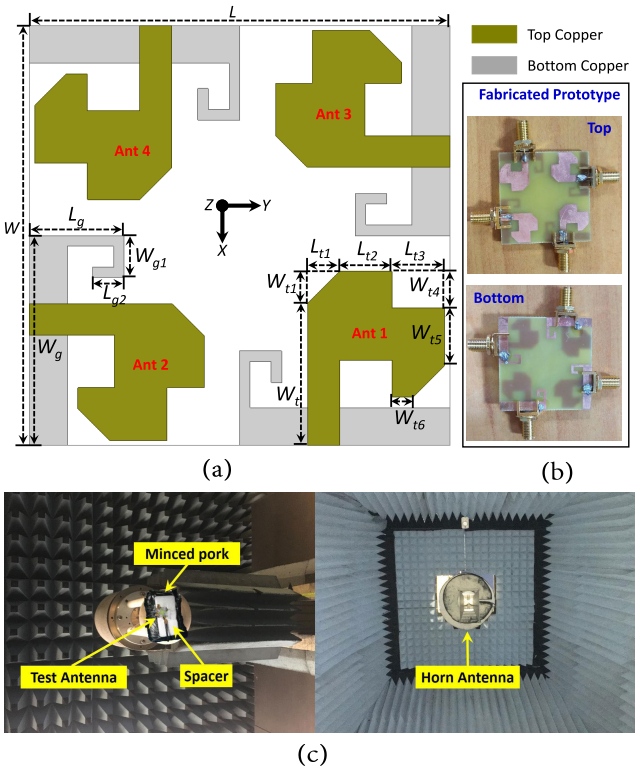

FIGURE 1. (a) Proposed wideband CP MIMO antenna [$W = L = 40$, $L_g = 9$, $W_g = 20$, $L_{g2} = 3$, $W_{g1} = 4$, $W_t = 13.6$, $W_{t1} = L_{t1} = 3$, $L_{t2} = L_{t3} = 5$, $W_{t4} = 3.5$, $W_{t5} = 5.5$, and $W_{t6} = 2$ ($Units = mm$)], (b) fabricated prototype, and (c) radiation pattern measurement setup.

The antenna is printed on a 1.6 mm FR-4 substrate ($\epsilon_r = 4.4$). The design model consists of four identical elements where each element is fed by a 50 Ω microstrip transmission line from one edge. The transmission line width is calculated using equations (1)-(2) [20]. The radiating structure is a modified square patch (SP). The modifications are done to attain miniaturization and to generate circular polarization (CP). The common methods to attain CP include truncating the corners of the patch, cutting the diagonal slots in the patch, and by using additional stubs and slits [17]. In this design, the CP is obtained by the truncated corner technique and the CP bandwidth is further enhanced by using an additional open circuited stub on the ground plane. The truncated corner patch and hook-shaped open circuited stub assisted in the production of two orthogonal modes of the same amplitude. The final results of the optimized antenna in terms of reflection coefficient (S_{11}), elements isolation, axial ratio are shown in Fig. 2. The antenna has an absolute bandwidth of 2.23 GHz (1.71–3.94 GHz), as shown in Fig. 2a. The antenna also retains the 3-dB CP bandwidth of 1.3 GHz (1.8–3.1 GHz), as illustrated in Fig. 2b. The MIMO system elements are fairly isolated from each other (transmission coefficient $<$ -24 dB) within the operating band, as given in Fig. 2c. The surface current distribution of the proposed antenna is portrayed in Fig. 2d. It is concluded from the directions of the J_{surf} fields that the proposed antenna exhibits a left-hand

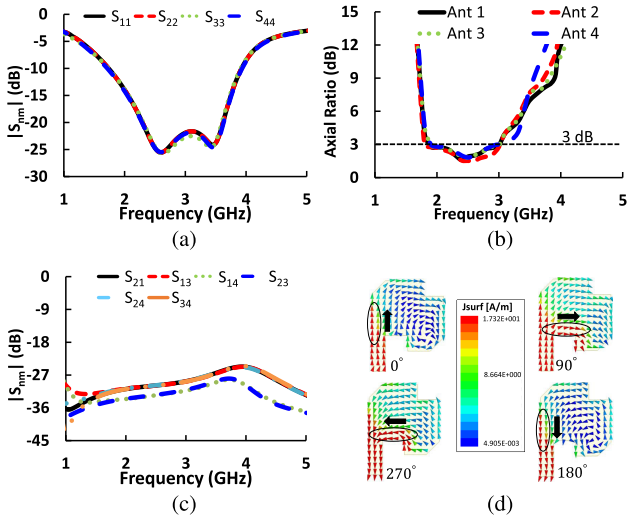

FIGURE 2. Simulated results (a) reflection coefficient, (b) axial ratio, (c) mutual coupling and (d) fields distribution at 2.4 GHz.

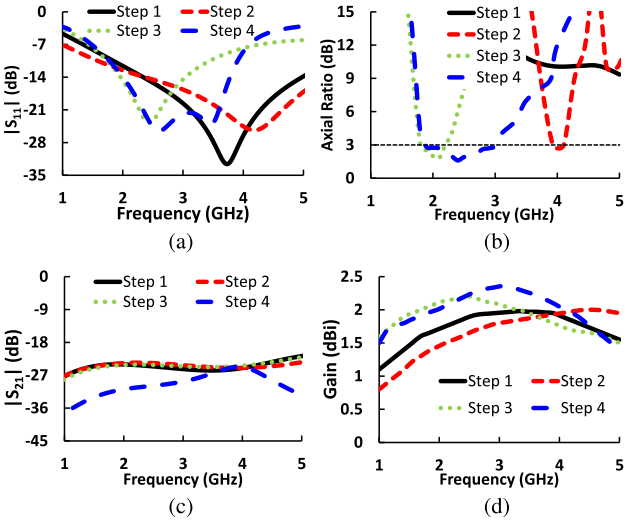

FIGURE 4. Antenna parameters in design evolution (a) reflection coefficient, (b) axial ratio, (c) mutual coupling, and (d) gain.

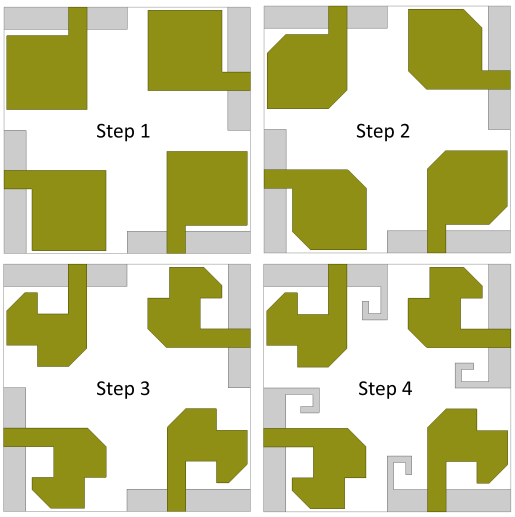

FIGURE 3. Design evolution of the wideband CP MIMO antenna.

circular polarization.

$$\epsilon_{eff} = \frac{\epsilon_r + 1}{2} + \frac{\epsilon_r - 1}{2}\left(1 + 12\frac{h}{W}\right)^{-0.5} \quad (1)$$

$$Z = \frac{120\pi}{\sqrt{\epsilon_{eff}}}\left[\frac{W}{h} + 1.393 + 0.677 \times ln\left(\frac{W}{h} + 1.444\right)\right]^{-1} \quad (2)$$

where ϵ_{eff} is the effective permittivity of the material, ϵ_r is the relative permittivity of the substrate, h is the substrate thickness and W is width of the transmission line.

A. DESIGN EVOLUTION

An iterative process for obtaining the desired results is consist of four steps as shown in Fig. 3. In the first iteration (step 1), SP is excited by a microstrip transmission line from one edge. In this iteration, the antenna resonated at 3.75 GHz with linear polarization. A 10-dB bandwidth (fractional bandwidth) of 3.81 GHz (102 % at the center frequency of 3.75 GHz) is achieved in the first iteration. The isolation of −23.6 dB is observed at 2.4 GHz in the first iteration. The peak gain is 1.98 dBi at 3.34 GHz. In the second stage, the SP is truncated at the edges. The linear polarization of the antenna is changed to circular polarization due to the truncated corners. In this step, the antenna resonated at 4.18 GHz with circular polarization (as shown in Fig. 4a and 4b). A 10-dB bandwidth (fractional bandwidth) of 4.78 GHz (114 % at the center frequency of 4.18 GHz) is achieved. The isolation of −24 dB is observed at 2.4 GHz in the second iteration. The peak gain is 1.99 dBi at 4.72 GHz. In the third stage, two rectangular sections are etched from the edge truncated SP. The rectangular slots produce an additional capacitance effect which shifted the resonant frequency to the lower frequency edge. In this iteration, the antenna resonated at 2.4 GHz with a circular polarization. A 10-dB bandwidth (fractional bandwidth) of 1.69 GHz (70 % at the center frequency of 2.4 GHz) is achieved in the third iteration. The isolation of −24.12 dB is observed at 2.4 GHz in third iteration. A 3-dB circular polarization bandwidth of 20 % at the center frequency of 2 GHz is observed, as illustrated in Fig. 4b. The peak gain is 2.22 dBi at 1.66 GHz. In the last iteration, a hook-shaped open-ended stub is connected to the ground plane to increase the antenna operational bandwidth and circular polarization bandwidth. In this stage, the proposed antenna has two resonances located at 2.5 and 3.47 GHz with a circular polarization. A 10-dB bandwidth (fractional bandwidth) of 2.21 GHz (92.1 % at the center frequency of 2.4 GHz) is achieved in the final iteration. The isolation of −30.1 dB is observed at 2.4 GHz in the final iteration. A 3-dB circular polarization bandwidth of 54.16 % (1.8–3.1 GHz) at the center frequency of 2.4 GHz is observed, as illustrated in Fig. 4b. The peak gain is 2.36 dBi at 2.1 GHz.

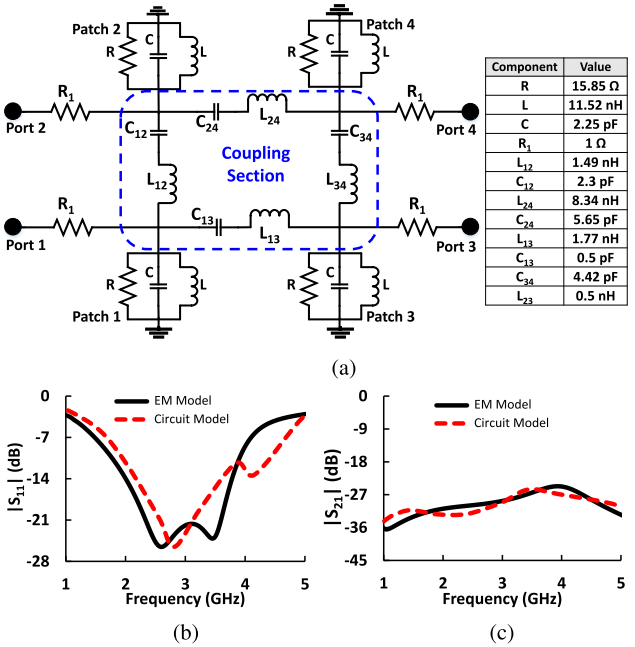

Component	Value
R	15.85 Ω
L	11.52 nH
C	2.25 pF
R_1	1 Ω
L_{12}	1.49 nH
C_{12}	2.3 pF
L_{24}	8.34 nH
C_{24}	5.65 pF
L_{13}	1.77 nH
C_{13}	0.5 pF
C_{34}	4.42 pF
L_{23}	0.5 nH

FIGURE 5. (a) Circuit model of the 4-element MIMO antenna, (b) $|S_{11}|$ comparison of the EM model and circuit model, and (c) $|S_{21}|$ comparison of the EM model and circuit model.

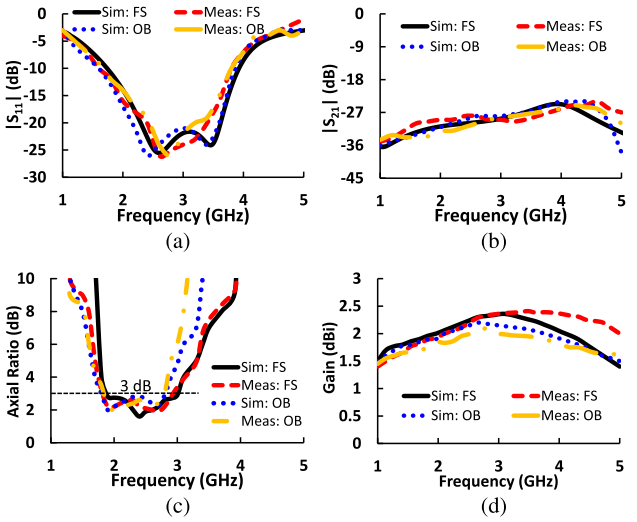

FIGURE 6. Simulated and measured results (Free Space = FS, On-body = OB) (a) $|S_{11}|$, (b) $|S_{21}|$, (c) axial ratio, and (d) gain.

B. EQUIVALENT CIRCUIT MODEL

Fig. 5a portrays the equivalent resonance circuit model for the four elements MIMO system where each element is represented by the RLC lumped component [21]. Each element is excited by a separate 50 Ω terminal. We know that there is always some coupling associated with the nearby Antennas. The coupling between the nearby antennas is modeled by LC series lumped elements [22]. The value of each component of the system is shown in Fig. 5a. The equivalent circuit model is simulated using ADS software. A comparison between S-parameter results of the full-wave electromagnetic model and the equivalent circuit model is shown in Fig. 5b-5c. The results of both models are well-matched within the desired band.

III. EXPERIMENTAL RESULTS AND DISCUSSIONS

The proposed antenna model is fabricated on a standard FR-4 substrate ($\epsilon_r = 4.4$, thickness = 1.6 mm). A photograph of the final antenna is shown in Fig. 1b. The antenna reflection coefficient, gain, axial ratio, radiation pattern, and MIMO parameters are measured. The impact of human body on performance of the antenna is also studied in terms of the aforementioned parameters. The antenna is placed on the right arm of the full-scale model of the human body. A 4 mm airgap is kept between the antenna and the arm of the human body while simulating the antenna.

A. REFLECTION AND TRANSMISSION COEFFICIENT

The simulated and measured antenna reflection coefficient ($|S_{11}|$, $|S_{22}|$, $|S_{33}|$, and $|S_{44}|$) in free space are shown in Fig. 6a ($|S_{22}|$, $|S_{33}|$, and $|S_{44}|$ are identical to $|S_{11}|$ and not shown for brevity). The simulated $|S_{11}|$ has two resonances at 2.56 and 3.47 GHz while the measured $|S_{11}|$ has one resonance at 2.6 GHz. The simulated and measured 10-dB bandwidths are 2210 MHz (1.73–3.94 GHz) and 2200 MHz (1.6–3.8 GHz), respectively. The simulated and measured 10-dB fractional bandwidths (FBW) are equal to 92.08 % and 91.66 % at the center frequency of 2.4 GHz, respectively. The antenna covered two major bands namely, the Industrial, Scientific, and Medical (ISM) band (2.40–2.48 GHz) and Worldwide Interoperability for Microwave Access (WiMAX) band (3.3–3.8 GHz). The achieved wide bandwidth can handle any fabrication tolerance and any detuning effect caused by the nearby electronic devices or human body. The $|S_{11}|$ of the antenna is also simulated and measured while placing the antenna on the right-arm of a full-scale model of the human body (Fig. 6a). The antenna resonates at slightly shifted lower frequencies due to high permittivity of the human body. It is noticed that the antenna bandwidth remains the same and maintains the wideband response at the targeted ISM band. The simulated and measured bandwidths of the antenna are 2200 MHz (1.6–3.8 GHz) and 1970 MHz (1.84–3.81 GHz, respectively. The simulated and measured 10-dB fractional bandwidths (FBW) are equal to 91.66 % and 82.08 % at the center frequency of 2.4 GHz, respectively.

The simulated and measured antenna transmission coefficient ($|S_{21}|$) in free space is shown in Fig. 6b. The simulated and measured $|S_{21}|$ are < -25 dB and < -25.3 dB, respectively within the operating frequency band (1.71–3.94 GHz). The simulated (measured) $|S_{21}|$ in on-body worn case is < -26 dB (< -26.5 dB) within the same operating frequency band, as shown in Fig. 6b.

B. AXIAL RATIO AND PEAK GAIN

The simulated and measured axial ratio (AR) of the antenna in free space is illustrated in Fig. 6c. The simulated AR is

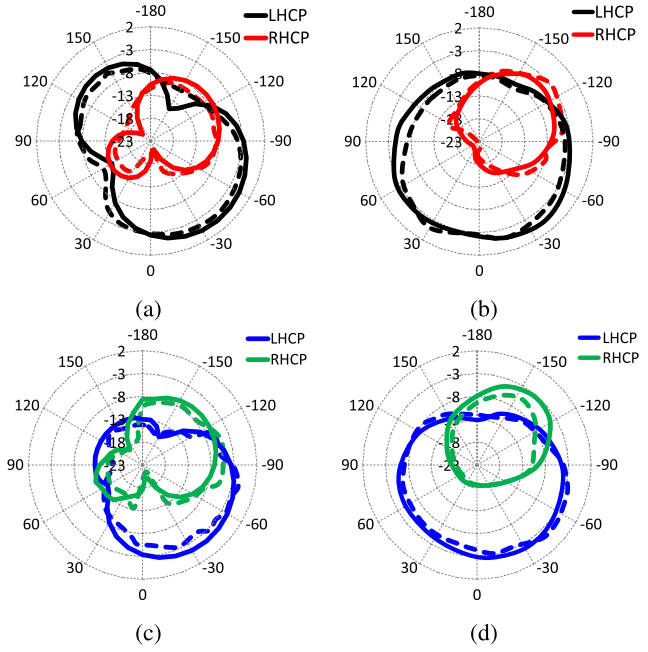

FIGURE 7. Simulated (solid line) and measured (dashed line) radiation pattern of the antenna at 2.4 GHz (a) $\phi = 0°$ (free space), (b) $\phi = 90°$ (free space), (c) $\phi = 0°$ (on body), (d) $\phi = 90°$ (on body).

less than 3 dB from 1.9 GHz to 3.2 GHz, covering a 3-dB AR bandwidth of 1300 MHz (FBW of 54.16 % at the center frequency of 2.4 GHz). The measured AR is less than 3 dB from 1.81 GHz to 3 GHz, covering a 3-dB AR bandwidth of 1190 MHz (FBW of 49.58 % at the center frequency of 2.4 GHz). The AR measurements agree well with simulations. The simulated and measured results of AR of the antenna as worn on the model are shown in Fig. 6c. The AR bandwidth of the antenna is reduced when worn on the human body. The simulated 3-dB AR bandwidth of the antenna is equal to 1040 MHz (1.8–2.84 GHz) with a 3-dB FBW of 43.33 %, while the measured AR bandwidth is equal to 940 MHz (1.86–2.8 GHz) with a 3-dB FBW of 39.16 %.

Fig. 6d portrays the simulated and measured peak gain of the antenna in free space versus frequency. The simulated peak gain has a maximum value of 2.36 dBi at 2.1 GHz. The simulated peak gain of the antenna lies between 1.96 and 2.36 dBi in the operational frequency band (1.71–3.94 GHz). The measured peak gain has a maximum value of 2.39 dBi at 3.75 GHz. The measured peak gain of the antenna lies between 1.89 and 2.39 dBi in the operational frequency band. Also, peak gain of the antenna is simulated and measured on human body. The simulated (measured) peak gain is $>$ 1.88 dBi ($>$ 1.75 dBi) in the operational band in on-body worn case.

C. RADIATION PATTERN

The radiation patterns [2-D left-hand circular polarization (LHCP) and right-hand circular polarization (RHCP)] of the antenna are measured in free space in two principal planes ($\phi = 0°$ and $\phi = 90°$) at 2.4 GHz. Fig. 7 shows that the simulated (measured) LHCP is greater than the RHCP by 19.1 dB (20.8 dB). Additionally, the radiation patterns are evaluated in on-body worn case. The simulated and measured antenna radiation patterns in both principle planes ($\phi = 0^0$ and $\phi = 90^0$) in on-body worn case at 2.4 GHz are compared in Fig. 7c–7d. The LHCP is predominated over the RHCP in both planes. The simulated (measured) LHCP is predominated over the RHCP by 18.06 dB (16.34 dB), as shown in Fig. 7. The results show that the antenna exhibits LHCP in free space as well as when worn on the human-body model.

D. ENVELOP CORRELATION COEFFICIENT (ECC)

The envelop correlation coefficient (ECC) is one of the important factors in determining the suitability of the MIMO antenna systems. The ECC determines the independency of elements in their individual performance. It is desirable for the ECC of the MIMO antenna system to have a zero value, but MIMO antenna systems with an ECC less than 0.5 are considered acceptable. The ECC can be evaluated from the S-parameter using Equation. (3) [23] or from the far-field radiation patterns using Equation. (4) [24]. In this paper, far-field radiation patterns are used to determine ECC of the system. The ECC between antenna 1 and rest of the antennas is calculated in free-space as well as on the human-body model, as shown in Fig. 8a. The ECC of the antenna in free space is less than 0.21 within the operating frequency band. Furthermore, the ECC of the antenna as worn on the human-body model is less than 0.23 within the operating frequency band. The low values of the ECC make this system suitable for wearing on human-body and in devices where high data rate is required.

$$ECC = \frac{|S_{11}^* S_{12} + S_{22}^* S_{21}|^2}{[1 - (|S_{11}|^2 + |S_{12}|^2)][1 - (|S_{22}|^2 + |S_{21}|^2)]} \quad (3)$$

$$ECC = \frac{|\int\int_{4\pi} (\vec{B}_i(\theta, \phi)) \times (\vec{B}_j(\theta, \phi))\, d\Omega|^2}{\int\int_{4\pi} |(\vec{B}_i(\theta, \phi))|^2\, d\Omega \int\int_{4\pi} |(\vec{B}_j(\theta, \phi))|^2\, d\Omega} \quad (4)$$

where S_{11}/S_{22} and S_{21}/S_{12} are the reflection and transmission coefficients of the antenna. $\vec{B}_i(\theta, \phi)$ is the three dimensional radiation pattern upon excitation of the i^{th} antenna and $\vec{B}_j(\theta, \phi)$ is the three dimensional radiation pattern upon excitation of the j^{th} antenna. Ω is the solid angle.

E. DIVERSITY GAIN (DG)

Another parameter related to the MIMO antenna system is the diversity gain (DG), which portrays impact of the diversity scheme on the transmitted power. The DG of the system can be evaluated using Equation. (5) [12].

$$DG = 10\sqrt{1 - (ECC)^2} \quad (5)$$

The simulated DG of the system in free space and when worn on the human-body model is illustrated in Fig. 8b. The DG of the system in free space (when worn on the model) is greater than 9.77 dB (9.71 dB) within the operational frequency band.

TABLE 1. Performance comparison with the on-body antennas.

Ref.	MIMO (Yes/No)	Polarization	Size (λ_g^2)	Bandwidth (MHz)/FBW (Free Space)	Bandwidth (MHz)/FBW (On-body)	CP Bandwidth (MHz)/FBW (Free Space)	CP Bandwidth (MHz)/FBW (On-body)	Gain (dBi) (Free Space)	Gain (dBi) (On-body)
[5]	No	Linear	0.80×0.45	120/4.88%	140/5.83%	–	–	6.88	7.43
[9]	Yes	Linear	0.34×0.34	∼480/20%	∼456/19%	–	–	2.79	1.67
[10]	Yes	Linear	0.64×0.40	9590/127%	Not Given	–	–	5.1	–
[11]	Yes	Linear	π×0.05	90/3.68%	Not Given	–	–	4.2	3
[14]	No	Circular	0.44×0.44	100/4.5%	∼100/4.5%	56/2.04%	60/2.4%	4.7	4.68
[15]	No	Circular	0.53×0.53	490/12.2%	∼490/12.2%	490/12.2%	∼490/12.2%	5.3	6.7
[16]	No	Circular	0.41×0.41	270/10.77%	Not Given	69/2.72%	Not Given	5.2	∼3.4
[17]	Yes	Circular	0.50×0.50	140/5.7%	Not Given	100/4.08%	Not Given	Not Given	Not Given
[18]	No	Dual	π×0.065	Not Given Not Given	320/10% 710/9%	Not Given –	2000/83.3% –	-5.1 3.3	Not Given Not Given
[19]	No	Dual	0.68×0.68	31/1.84% 17/0.74%	Not Given Not Given	12/0.69% –	Not Given –	5.1 5.03	5.1 5.03
This work	**Yes**	**Circular**	**0.67×0.67**	**2210/92.08%**	**2200/91.66%**	**1300/54.16%**	**1040/43.33%**	**1.96–2.36**	**1.88–2.18**

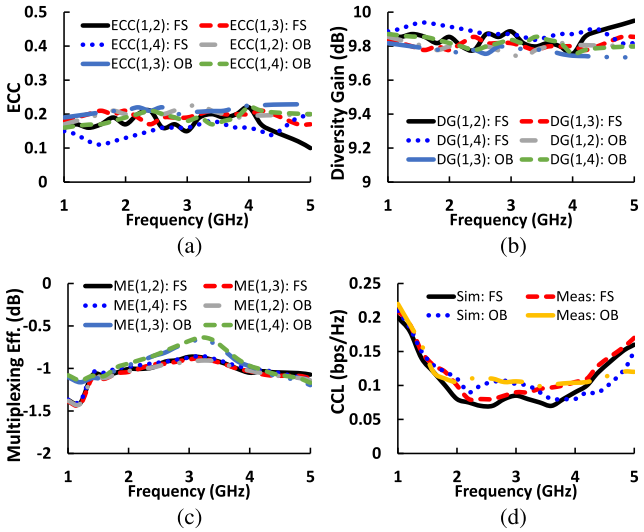

FIGURE 8. Diversity results (a) ECC, (b) diversity gain, (c) multiplexing efficiency, and (d) CCL.

F. MULTIPLEXING EFFICIENCY (ME)

The multiplexing efficiency (ME) of the antenna is calculated using Equation. (6) [25].

$$\eta_{Mux} = \sqrt{(1 - |\rho|^2)\eta_1\eta_2} \tag{6}$$

where η_{Mux} represents ME, and η_1 represents the efficiency of antenna 1, η_2 shows the efficiency of antenna 2 and ρ shows the complex ECC. Fig. 8c portrays the simulated ME of the antenna in free space and as worn on the human-body model. The ME of the antenna in free space is between −0.85 dB and −1.01 dB within the operating frequency band. Also, the ME of the antenna in on-body worn case is between −0.63 dB and −1.04 dB within the operating frequency band.

G. CHANNEL CAPACITY LOSS (CCL)

The channel capacity loss (CCL) of the MIMO antenna system is calculated using Equation. (7) [26]. The simulated and measured antenna CCL in free space and in on-body worn scenario is illustrated in Fig. 8d. The simulated and measured CCL results in free space are 0.07–0.1 bps/Hz and 0.08–0.13 bps/Hz within the operating frequency band. Also, the simulated and measured CCL results of the MIMO system in on-body worn case are 0.09–0.13 bps/Hz and 0.103–0.13 bps/Hz within whole operating frequency band. It is found that the CCL values of the system are within the limit (< 0.5 bps/Hz [21]) in free space as well as in on-body worn case, which confirms its suitability for use in MIMO system.

$$CCL = -log_2 \det(\Psi_{ant}) \tag{7}$$

where Ψ_{ant} is the correlation matrix of the antenna and it is given by

$$\Psi_{ant} = \begin{bmatrix} \rho_{11} & \rho_{12} & \rho_{13} & \rho_{14} \\ \rho_{21} & \rho_{22} & \rho_{23} & \rho_{24} \\ \rho_{31} & \rho_{32} & \rho_{33} & \rho_{34} \\ \rho_{41} & \rho_{42} & \rho_{43} & \rho_{44} \end{bmatrix} \tag{8}$$

where

$$\rho_{ii} = 1 - \Big|\sum_{n=1}^{n=4} S_{in}^* S_{ni}\Big|, \quad for\ i, j = 1, 2, 3, or\ 4.$$

and

$$\rho_{ij} = -\Big|\sum_{n=1}^{n=4} S_{in}^* S_{nj}\Big|, \quad for\ i, j = 1, 2, 3, or\ 4.$$

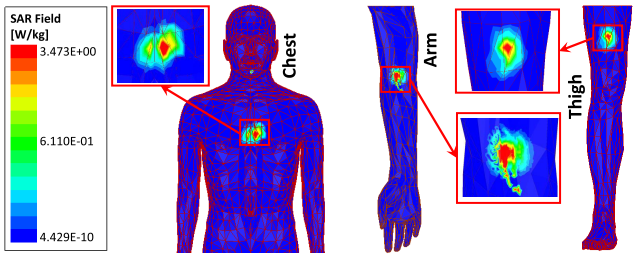

FIGURE 9. 10-g Specific absorption rate distributions at 2.4 GHz on the chest, arm and thigh of the body.

IV. SPECIFIC ABSORPTION RATE (SAR) ANALYSIS

In order to evaluate the specific absorption rate (SAR), the antenna is placed on the right arm of a full-scale model of the human body. A 4 mm airgap is kept between the antenna and arm of the model while simulating the antenna. The human body absorbs the backward electromagnetic radiations [at what is called the specific absorption rate (SAR)] of the antenna when it is operated in the environs. The temperature of the tissues can rise due to excessive absorption (beyond healthy limits) of these electromagnetic radiations. Keeping in mind the concern for wearer safety, the regulatory authorities (FCC, IEEE and ICNIRP) standardized the SAR limits. With the same concern in mind, SAR values are set according to IEEE C95.1-2005 standards. The SAR levels are evaluated on the chest, right arm, and right thigh of the human model. For all three positions, the 10-g peak SAR value of 3.473 W/Kg is noted for 1 W of input power and shown in Fig. 9. Most of the devices that operate in the environs of the human body use little power (mW range). To restrict the SAR value under our limits in the proposed antenna, its maximum input power must be 575.87 mW, which is above the limit. Based on the above SAR calculated value, the proposed antenna is safe if the input power is less than 575.87 mW.

A. LINK BUDGET ANALYSIS

To analyze effectiveness of the designed antenna, it is analyzed based on two different cases. In the first case, we analyzed the power transmitting ability of the antenna when it is worn on the human body. In this case the receiving antenna is located away in free space. In the second case, we considered the communication between an implantable device and our designed wearable antenna.

1) CASE 1

In this case our proposed antenna acted as a transmitting antenna while it is placed above the human body and an ideal $\lambda/2$ dipole antenna acted as an antenna to receive the transmitted power. We keep the distance a between our antenna and the $\lambda/2$ dipole antenna. Equation. (9) is used to calculate the power at the receiving end [14].

$$P_{ra}(dBm) = P_t(dBm) + G_{ta}(dB) + G_{ra}(dB) - PL(dB) \quad (9)$$

TABLE 2. Performance comparison of the antenna in free space and on-body worn scenario.

Parameters	Free Space (Simulated)	On-Body (Simulated)
Bandwidth (MHz)/FBW	2210/92.08%	2200/91.66%
Isolation (dB)	<-25	<-26
3-dB CP Bandwidth (MHz)/FBW	1300/54.16%	1040/43.33%
Peak Gain (dBi)	1.96–2.36	1.88–2.18
Envelop Correlation Coefficient	<0.21	<0.23
Diversity Gain (dB)	9.77	9.71
Multiplexing Efficiency (dB)	-0.85	-0.63
Channel Capacity Loss (bps/Hz)	0.07–0.1	0.09–0.13

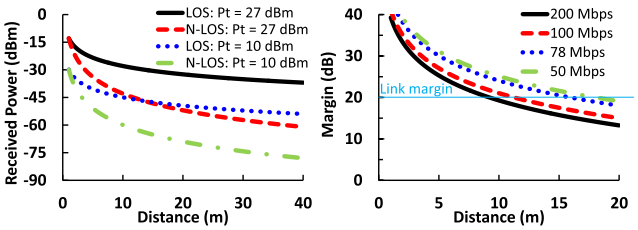

FIGURE 10. (a) Power received by the antenna in on-body worn scenario (LOS and N-LOS), and (b) link margin against varying data rates and distance.

where $P_{ra}(dBm)$ is the receiving power for ideal dipole antenna in dBm, $P_t(dBm)$ is the transmitted power by our CP MIMO antenna in dBm, $G_{ta}(dB)$ is the gain of our CP MIMO antenna in dB, $G_{ra}(dB)$ is the gain of an ideal $\lambda/2$ dipole antenna in dB, and $PL(dB)$ is the distance dependent path loss in dB. We used Equation. (10) to compute the $PL(dB)$ [14].

$$PL(dB) = 10\gamma log_{10}\left(\frac{a}{a_\circ}\right) + 20log_{10}\left(\frac{4\pi a_\circ}{\lambda_\circ}\right) + X_\sigma \quad (10)$$

where γ is the path loss exponent. The value of γ depends on the nature of communication. The value of γ is 1.5 and 3 for line of sight (LOS) and non-line of sight communication (N-LOS), respectively. The distance between the proposed antenna (transmitting antenna) and the ideal $\lambda/2$ dipole antenna (receiving antenna) is represented as a, $a_\circ$ is the reference distance of 1 m [27]- [28], $\lambda_\circ$ is the free space wavelength calculated at 2.4 GHz and X_σ is the shadowing factor for Gaussian distribution with a standard deviation of σ. We keep the transmitting power (P_t) value of 10 dBm and 27 dBm under the assumption that the antenna is mounted on the human body. The gain of the receiving antenna (G_{ra}) is chosen as 2 dBi.

It is found that receiving power of the antenna in the LOS scenario is better than N-LOS. It is also found that the receiving power (P_{ra}) is increasing with the transmitting power (P_t), as illustrated in Fig. 10a. In LOS communication, the power received by the receiving antenna is better than -37 dBm

TABLE 3. Parameters of link budget.

Transmission (Implantable device)	
Polarization	LHCP
Transmitting power (P_{t1})	-5 dBm
Transmitting antenna gain (G_{t1})	-27 dBi
Propagation	
Distance	1-20 m
Free-space loss (L_f)	Distance dependent
Receiver (wearable antenna)	
Polarization	LHCP
Receiver antenna gain (G_{ra})	2.1 dBi
Temprature	273 K
Boltzmann constant	1.38×10^{-23}
Noise power density ($N_\circ$)	-203.9 dB/Hz
Signal Quality	
Bit rate (B_r)	50, 78, 100, 200 Mbps
Bit error rate	1×10^{-5}
E_b/N_0 (ideal PSK)	9.6 dB
Margin (dB) = A_p–B_p	

and −54 dBm even at a separation of 40 m for the transmitting power of 27 dBm and 10 dBm, respectively. In the N-LOS communication, the power received by the antenna is better than −65 dBm at a separation of 15 m from the body worn antenna, when the transmitted power is 10 dBm. With the increase in the transmitted power (P_t = 27 dBm), the power received by the antenna is better than −65 dBm at a distance of 40 m. As a conclusion from this analysis, the proposed antenna satisfies the minimum sensitivity of ISM receivers [29].

2) CASE 2

In this case, down-link communication is assumed, where implantable antenna of the biomedical device is a transmitting antenna and the proposed wearable antenna is a receiving antenna. The link budget parameters are listed in Table. 3. The required receive power of the wearable antenna can be found using Equation. (11) [30]. The available antenna power from the implantable device can be derived from Equation. (12) [30].

$$B_p(dB) = \frac{E_b}{N_\circ} + kT_\circ + B_r \tag{11}$$

$$A_p = P_{t1}(dBm) + G_{t1}(dBi) + G_{r1}(dBi) - PL(dB) - L_f(dB) \tag{12}$$

where

$$L_f = 20log_{10}\left(\frac{4\pi a}{\lambda}\right) \tag{13}$$

The authors of [30]–[32] proposed that the margin between the B_p and A_p should be at least 20-25 dB for quality communication. The link margin against several distances and data rates is plotted in Fig. 10b. It is noticed that the margin is decreasing with the distance and data rates. It is also noticed that reliable communication is possible up to a distance of 10 m for the highest data rate of 200 Mbps. The reliable communication of our antenna with the implantable devices even at the highest data rate of 200 Mbps confirms the suitability of our antenna for high data rates biotelemetric devices.

The performance of the proposed antenna is compared with published wearable antennas in Table. 1. The proposed antenna exhibits a greater 10-dB bandwidth in free space and in on-body worn situation. Additionally, it has a wider 3-dB CP bandwidth in both conditions.

V. CONCLUSION

In this paper, a wideband circularly polarized MIMO antenna for high data wearable biotelemetric devices is designed and measured. The MIMO system includes four microstrip antennas with the same shape and size and they are placed orthogonally to adjacent elements. A wider 10-dB bandwidth is obtained for antenna in free space and in on-body worn case. Also, the 3-dB CP bandwidth is 1300 MHz in free space and 1040 MHz in on-body worn scenario. Additionally, the antenna peak gain, efficiency, ECC, DG, CCL and ME are satisfied on the human-body and in free space. The SAR value is in limit (for the input power of <575.87 mW) which confirms safety of the antenna for use in on-body communication. The link budget shows suitability of the antenna for high date rates over a reasonable area.

REFERENCES

[1] P. S. Hall, *Antennas and Propagation for Body-centric Wireless Communications*. Norwood, MA, USA: Artech House, 2012.

[2] S. Yan, P. J. Soh, and G. A. E. Vandenbosch, "Wearable ultrawideband technology—A review of ultrawideband antennas, propagation channels, and applications in wireless body area networks," *IEEE Access*, vol. 6, pp. 42177–42185, 2018.

[3] Y. Hao, A. Alomainy, P. S. Hall, Y. I. Nechayev, C. G. Parini, and C. C. Constantinou, "Antennas and propagation for body centric wireless communications," in *Proc. IEEE/ACES Int. Conf. Wireless Commun. Appl. Comput. Electromagn.*, Apr. 2005, pp. 586–589.

[4] S. Hong, S. H. Kang, Y. Kim, and C. W. Jung, "Transparent and flexible antenna for wearable glasses applications," *IEEE Trans. Antennas Propag.*, vol. 64, no. 7, pp. 2797–2804, Jul. 2016.

[5] M. A. B. Abbasi, S. S. Nikolaou, M. A. Antoniades, M. N. Stevanovic, and P. Vryonides, "Compact EBG-backed planar monopole for BAN wearable applications," *IEEE Trans. Antennas Propag.*, vol. 65, no. 2, pp. 453–463, Feb. 2017.

[6] Y.-S. Chen and T.-Y. Ku, "A low-profile wearable antenna using a miniature high impedance surface for smartwatch applications," *IEEE Antennas Wireless Propag. Lett.*, vol. 15, pp. 1144–1147, 2016.

[7] R. Chavez-Santiago, I. Balasingham, and J. Bergsland, "Ultrawideband technology in medicine: A survey," *J. Elect. Comput. Eng.*, vol. 2012, pp. 1–9, 2012.

[8] A. Kiourti, K. A. Psathas, and K. S. Nikita, "Implantable and ingestible medical devices with wireless telemetry functionalities: A review of current status and challenges," *Bioelectromagnetics*, vol. 35, no. 1, pp. 1–15, Jan. 2014.

[9] H. Li, S. Sun, B. Wang, and F. Wu, "Design of compact single-layer textile MIMO antenna for wearable applications," *IEEE Trans. Antennas Propag.*, vol. 66, no. 6, pp. 3136–3141, Jun. 2018.

[10] A. Kumar Biswas and U. Chakraborty, "Compact wearable MIMO antenna with improved port isolation for ultra-wideband applications," *IET Microw., Antennas Propag.*, vol. 13, no. 4, pp. 498–504, Mar. 2019.
[11] D. Wen, Y. Hao, M. O. Munoz, H. Wang, and H. Zhou, "A compact and low-profile MIMO antenna using a miniature circular high-impedance surface for wearable applications," *IEEE Trans. Antennas Propag.*, vol. 66, no. 1, pp. 96–104, Jan. 2018.
[12] A. Iqbal, O. A. Saraereh, A. W. Ahmad, and S. Bashir, "Mutual coupling reduction using F-shaped stubs in UWB-MIMO antenna," *IEEE Access*, vol. 6, pp. 2755–2759, 2018.
[13] J. Zhu, S. Li, B. Feng, L. Deng, and S. Yin, "Compact dual-polarized UWB quasi-self-complementary MIMO/diversity antenna with band-rejection capability," *IEEE Antennas Wireless Propag. Lett.*, vol. 15, pp. 905–908, 2016.
[14] Z. H. Jiang, M. D. Gregory, and D. H. Werner, "Design and experimental investigation of a compact circularly polarized integrated filtering antenna for wearable biotelemetric devices," *IEEE Trans. Biomed. Circuits Syst.*, vol. 10, no. 2, pp. 328–338, Apr. 2016.
[15] Z. H. Jiang and D. H. Werner, "A compact, wideband circularly polarized co-designed filtering antenna and its application for wearable devices with low SAR," *IEEE Trans. Antennas Propag.*, vol. 63, no. 9, pp. 3808–3818, Sep. 2015.
[16] Z. H. Jiang, Z. Cui, T. Yue, Y. Zhu, and D. H. Werner, "Compact, highly efficient, and fully flexible circularly polarized antenna enabled by silver nanowires for wireless body-area networks," *IEEE Trans. Biomed. Circuits Syst.*, vol. 11, no. 4, pp. 920–932, Aug. 2017.
[17] L. Qu, H. Piao, Y. Qu, H.-H. Kim, and H. Kim, "Circularly polarised MIMO ground radiation antennas for wearable devices," *Electron. Lett.*, vol. 54, no. 4, pp. 189–190, Feb. 2018.
[18] S. Bhattacharjee, S. Maity, S. R. B. Chaudhuri, and M. Mitra, "A compact dual-band dual-polarized omnidirectional antenna for on-body applications," *IEEE Trans. Antennas Propag.*, vol. 67, no. 8, pp. 5044–5053, Aug. 2019.
[19] K. N. Paracha, S. K. A. Rahim, P. J. Soh, M. R. Kamarudin, K.-G. Tan, Y. C. Lo, and M. T. Islam, "A low profile, dual-band, dual polarized antenna for indoor/outdoor wearable application," *IEEE Access*, vol. 7, pp. 33277–33288, 2019.
[20] C. A. Balanis, *Antenna Theory: Analysis and Design*. Hoboken, NJ, USA: Wiley, 2016.
[21] A. Iqbal, O. A Saraereh, A. Bouazizi, and A. Basir, "Metamaterial-based highly isolated MIMO antenna for portable wireless applications," *Electronics*, vol. 7, no. 10, p. 267, Oct. 2018.
[22] A. Iqbal, A. Bouazizi, S. Kundu, I. Elfergani, and J. Rodriguez, "Dielectric resonator antenna with top loaded parasitic strip elements for dual-band operation," *Microw. Opt. Technol. Lett.*, vol. 61, no. 9, pp. 2134–2140, Sep. 2019.
[23] J. Iqbal, U. Illahi, M. I. Sulaiman, M. M. Alam, M. M. Suud, and M. N. M. Yasin, "Mutual coupling reduction using hybrid technique in wideband circularly polarized MIMO antenna for WiMAX applications," *IEEE Access*, vol. 7, pp. 40951–40958, 2019.
[24] N. Hussain, M.-J. Jeong, J. Park, and N. Kim, "A broadband circularly polarized Fabry–Perot resonant antenna using a single-layered PRS for 5G MIMO applications," *IEEE Access*, vol. 7, pp. 42897–42907, 2019.
[25] A. Iqbal, A. Basir, A. Smida, N. K. Mallat, I. Elfergani, J. Rodriguez, and S. Kim, "Electromagnetic bandgap backed millimeter-wave MIMO antenna for wearable applications," *IEEE Access*, vol. 7, pp. 111135–111144, 2019.
[26] W. Wu, B. Yuan, and A. Wu, "A quad-element UWB-MIMO antenna with band-notch and reduced mutual coupling based on EBG structures," *Int. J. Antennas Propag.*, vol. 2018, pp. 1–10, 2018.
[27] A. Sani, A. Alomainy, and Y. Hao, "Numerical characterization and link budget evaluation of wireless implants considering different digital human phantoms," *IEEE Trans. Microw. Theory Techn.*, vol. 57, no. 10, pp. 2605–2613, Oct. 2009.
[28] Q. H. Abbasi, A. Sani, A. Alomainy, and Y. Hao, "Numerical characterization and modeling of subject-specific ultrawideband body-centric radio channels and systems for healthcare applications," *IEEE Trans. Inform. Technol. Biomed.*, vol. 16, no. 2, pp. 221–227, Mar. 2012.
[29] P. Roshan and J. Leary, *802.11 Wireless LAN Fundamentals*. San Jose, CA, USA: Cisco Press, 2004.
[30] R. Das and H. Yoo, "A wideband circularly polarized conformal endoscopic antenna system for high-speed data transfer," *IEEE Trans. Antennas Propag.*, vol. 65, no. 6, pp. 2816–2826, Jun. 2017.
[31] I. Gani and H. Yoo, "Multi-band antenna system for skin implant," *IEEE Microw. Wireless Compon. Lett.*, vol. 26, no. 4, pp. 294–296, Apr. 2016.
[32] A. Basir and H. Yoo, "A stable impedance-matched ultrawideband antenna system mitigating detuning effects for multiple biotelemetric applications," *IEEE Trans. Antennas Propag.*, vol. 67, no. 5, pp. 3416–3421, May 2019.

AMJAD IQBAL (Student Member, IEEE) received the degree in electrical engineering from the COMSATS Institute of Information Technology, Islamabad, Pakistan, in 2012, and the M.S degree in electrical engineering from the Department of Electrical Engineering, CECOS University of IT and Emerging Science, Peshawar, Pakistan, in 2018. He is currently pursuing the Ph.D. degree with the Faculty of Engineering, Multimedia University, Cyberjaya, Selangor, Malaysia. He worked as a Lab Engineer at the Department of Electrical Engineering, CECOS University, from 2016 to 2018. His research interests include printed antennas, flexible antennas, implantable antennas, MIMO antennas, dielectric resonator antennas, and synthesis of microwave components.

AMOR SMIDA (Member, IEEE) received the degree in electronic baccalaureate, in 2008, the M.Sc. degree in analyze and digital processing of the electronic systems, in 2010, and the Ph.D. degree, in 2014, from the Faculty of Mathematical, Physical and Natural Sciences of Tunis, Tunis El-Manar University, Tunisia. From 2008 to 2014, he was a Graduate Student Researcher with the Unit of Research in High Frequency Electronic Circuits and Systems. Since August 2014, he has been an Assistant Professor with the Department of Medical Equipment Technology, College of Applied Medical Sciences, Majmaah University, Saudi Arabia. His current researches focus on smart antennas, biosensors, biomedical applications, neural network applications in antennas, adaptive arrays. and microwave circuits design CST studio microwave.

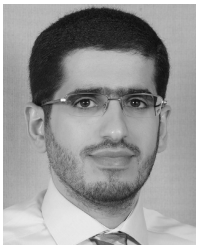

ABDULLAH J. ALAZEMI (Member, IEEE) received the B.S. degree in electrical engineering from Kuwait University, in 2010, and the M.S. and Ph.D. degrees in electrical and computer engineering from The University of California at San Diego, La Jolla, CA, USA, in 2013 and 2015, respectively. He joined the Department of Electrical Engineering, Kuwait University, where he is currently an Assistant Professor. His works focus on tunable antennas and filters with RF-MEMS, multiband power dividers and couplers for advanced communication systems, and MM-wave to THz Quasi-optical systems.

MOHAMED I. WALY received the degree in biomedical engineering and system baccalaureate, in 2004, the M.Sc. degree in biomedical engineering and system, in 2009, and the Ph.D. degree, in 2013, from the Faculty of Biomedical engineering and System, Cairo University, He was a Consultant Engineering with CASBEC, from 2013 to 2015. Since October 2015, he has been an Assistant Professor with the Department of Medical Equipment Technology, College of Applied Medical Sciences, Majmaah University, Saudi Arabia. His current researches focus on smart antennas, biosensors, biomedical applications, machine learning applications in medical field, mechanics, biomechanics applications, and predication disease model.

NAZIH KHADDAJ MALLAT (Senior Member, IEEE) received the B.Eng. (electrical and electronics engineering) degree from Lebanese University, Lebanon, in 2000, the master's degree from the Ecole Nationale Supérieure des Télécommunications de Bretagne (ENSTB), France, in 2002, and the Ph.D. degree in telecommunications from the University of Quebec, Institut National de la Recherche Scientifique (INRS), Canada, in 2010. After his Ph.D. and until January 2012, he held a postdoctoral fellowship at the Ecole Polytechnique de Montreal. In 2013, he joined the College of Engineering, Al Ain University (AAU), UAE, as an Assistant Professor, and was promoted to Associate Professor, in 2019. He was the Head of the Networks and Communication Engineering and Computer Engineering Department, from 2013 to 2017, the Deputy Dean of the College of Engineering, from 2014 to 2015, and the Dean of the College of Engineering, from September 2015 to March 2018, and has been the Director of the Quality Assurance and Institutional Research Center, since April 2018. He has acquired extensive teaching experience at both undergraduate and graduate levels. He has effectively taught many courses, and their relevant practical elements in laboratories at multiple Montreal universities (ETS, TELUQ, and Ecole Polytechnique de Montreal). His main research interests are passive microwave/millimeter-wave circuit, antennas, and telecommunications systems, where he authored or coauthored over 50 publications. The Fonds Québécois de la Recherche sur la Nature et les Technologies-FQRNT, a granting agency of the Quebec government, has awarded him two prestigious scholarships for his doctoral studies, in 2008, and postdoctoral research, from 2010 to 2011, thanks to his highest level of achievement. He was the Vice-Chair of the IEEE Montreal Section, from 2007 to 2008, Membership Development Chair, from 2009 to 2010, and Section Chair, from 2011 to 2012. He has served in the steering committee of many IEEE international conferences. He was the IEEE UAE Technical Activities Coordinator, from 2015 to 2018, and the IEEE Region 8 Chapter Coordination Subcommittee Chair, from 2015 to 2016. He was the Organizing Committee Chair of three major events held at Al Ain University: The 1st IEEE International Workshop at AAU, in February 2014, the 11th IEEE UAE Student Day, in May 2016, and the 16th Mediterranean Microwave Symposium (MMS), in November 2016. He is the Founder of the IEEE AAU Student Branch and the IEEE UAE MTT-S Chapter, and later the IEEE UAE MTT-S & IM-S & AP-S Joint Chapter.

SUNGHWAN KIM received the B.S., M.S., and Ph.D. degrees from Seoul National University, South Korea, in 1999, 2001, and 2005, respectively. He was a Postdoctoral Visitor with the Georgia Institute of Technology (GeorgiaTech), from 2005 to 2007, and a Senior Engineer with Samsung Electronics, from 2007 to 2011. He is currently an Associate Professor with the School of Electrical Engineering, University of Ulsan, South Korea. His main research interests are channel coding, modulation, massive MIMO, visible light communication, and quantum information.